Evaluating the Climate Change Trends and Spatiotemporal Variations of Evapotranspiration: A Case Study in El-Beheira Governorate, Egypt

Randa S. Makar [a*], Shuo Li [b] and Sahar A. Shahin [a]

[a] *Soils and Water Use Department, Agricultural and Biological Research Institute, National Research Centre, Egypt.*
[b] *Key Laboratory for Geographical Process Analysis and Simulation of Hubei Province, College of Urban and Environmental Sciences, Central China Normal University, Wuhan 430079, China.*

Authors' contributions

This work was carried out in collaboration among all authors. Author RSM designed the study and wrote the protocol. Authors RSM and SL wrote the first draft of the manuscript and managed the analyses of the study. Authors RSM and SAS performed the image and statistical analysis and managed the literature search. Author SAS did field work. All authors read and approved the final manuscript.

Original Research Article

ABSTRACT

Aims: Evapotranspiration (ET) is crucial for determining crop water requirements, while climate change and global warming are major concerns. Therefore, in this study, we aimed at evaluating the climate change trends and the spatiotemporal variations in ET in a selected area located in El-Beheira Governorate, Egypt, while accounting for potential land use/land cover (LULC) changes.
Methodology: We analyzed three Landsat images acquired in 1984, 2001, and 2020 to assess LULC changes in the study area. Climate change was studied from 1984 to 2021 using data from

NASA's Prediction of Worldwide Energy Resource (POWER) project. We also used the Terra MODIS MOD16A3GF Version 6.1 ET product from 2000 to 2021 to evaluate the spatiotemporal variations of ET.

Results: LULC change detection showed that the unchanged agricultural area from 1984 to 2020 accounted for 29.3% of the study area and was used to evaluate the changes of ET. Evaluating climate change revealed that there was an increased trend in temperature, relative humidity (RH), and precipitation, while no change was observed in wind speed. Similarly, the anomalies changes of temperature, RH, and precipitation had an increasing trend while wind speed was constant. On the other hand, the yearly ET values calculated from 2000 to 2021 had an increasing trend. There was a moderate correlation between RH and precipitation, as well as between ET and precipitation.

Conclusion: The increased trends in climatic parameters such as temperature will eventually require changes in crop patterns to adjust to these changes and maintain a profitable yield. Furthermore, the increase in ET will result in an increase in crop water requirements, which is problematic, especially considering the limited water resources in Egypt.

1. INTRODUCTION

Global warming is evident from observations of increases in average air and ocean temperatures (IPCC 2007). The release of greenhouse gases, primarily due to human activities, caused the global surface temperature to rise during the period of 2011-2020 by 1.1°C above the levels recorded between 1850 and 1900. Moreover, the global surface temperature has increased faster since 1970 than in any other 50-year period over the last 2000 years [2]. According to [1], the anticipated rise in temperature is projected to fall within a range of 1.2°C to 4.1°C by 2100, increasing to 1.9°C to 5.6°C by 3000. The increase in temperature would increase evaporation and affect hydrological processes [3]. Therefore, climate change has been acknowledged as one of the greatest challenges for humanity [4], and its impacts on agriculture and water resources have became a global concern [5], especially, concerning crop water supply and demand in many of the world's agricultural regions [6] and global food security [7]. Furthermore, water scarcity is considered a threat in many parts of the world [8], particularly most of the Mediterranean region, which is characterized by a semi-arid climate and chronic water scarcity and where agriculture consumes most of the water resources [9]. This region is characterized by insufficient rainfall to compensate for the evaporative losses by crops, as most of the available water is lost through evapotranspiration,and water availability is considered a major limitation of crop production [10].

Evapotranspiration, the water vapor flux transported from land to air [11], is an important component of global water, carbon, and energy cycles [12], and plays a key role in estimating crop water requirements and future planning in context with agricultural and water management [13]. Therefore, continuous monitoring of ET is considered critical for water resource management at both regional and local scales [14]. The direct estimation of ET is rather complicated particularly, with sparse data availability [15]. On the other hand, satellite remote sensing provides spatially and temporally continuous information that can be used for global indirect ET estimation [12]. Many of these satellite remote sensing based-ET products can be retrieved from various remote sensing platforms, such as the Moderate Resolution Imaging Spectroradiometer (MODIS) ET product, which has been released since 2000 by the National Aeronautics and Space Administration (NASA) [16].

Moreover, land use/ land cover change and climate change were identified as the two factors increasingly affecting ET [17]. For example, forest loss increased surface albedo, reduced leaf area index, and decreased ET [18]. On the other hand, an increase in irrigated vegetation cover leads to increased water consumption through evapotranspiration and excess evaporation caused by the storage of water for irrigation [3]. Nevertheless, climate change was more influential than LULC change in affecting ET [19]. Several climatic parameters can influence ET. Decreasing humidity and increasing temperature, solar radiation, and wind speed can increase ET [4]. Nevertheless, ET is more sensitive to the increase in temperature than to the increase in net solar radiation [20] and wind speed [21]. As temperature increase

due to climate change, there will be a higher amount of energy available to vaporize the liquid water and consequently increasing the rate of ET [22]. The aim of this research is to evaluate the climate change trends and spatiotemporal evapotranspiration changes in a selected agricultural area in El-Beheira Governorate, Egyptthat has undergone no LULC change since 1984.

2. MATERIALS AND METHODS

2.1 Study area

The study area is located in El-Beheira Governorate, Egypt. The area is outlined by latitudes 30°29'24" and 30°56'55" N and longitudes 29°43'48" and 30°31'12"E(Fig. 1). It has a total area of 1112.8 km^2 and is bounded by the district boundary, El-Nubariya irrigation canal, and Cairo–Alexandria dessert road. According to Ebaid et al.[23], El-Beheira governorate is characterized by an annual mean temperature of 21 °C, relative humidity of 57%, wind speed of 350 km/day and rainfall between 9.6 and 24.8 mm/month occurring from November to February. Since 1980, the area has experienced considerable land use/land cover (LULC) changes due to the reclamation of its southern part.

2.2 Remote Sensing Data Collection and Processing

2.2.1 Landsat data

In this study, Landsat satellites were used to determine the LULC pattern and changes in the study area. Three images acquired on 11/9/1984, 23/12/2001 and 30/9/2020 from Landsat-5, Landsat-7 and Landsat-8 satellites, respectively, were used. The images were freely available online via https://earthexplorer.usgs.gov (accessed on 26-28/2/2022). These top of atmosphere (TOA), atmospherically corrected surface reflectance data were geometrically corrected and projected into Universal Transverse Mercator (UTM) and World Geodetic System 1984 (WGS 84) with datum-zone 36 N. The Landsat-8 Operational Land Imager (OLI) sensor had improved calibration, signal to noise characteristics, higher radiometric resolution, and spectrally narrower wavebands compared to the Landsat-7 Enhanced Thematic Mapper (ETM+) sensor [24]. Whereas the least developed was the Landsat 5 Thematic Mapper (TM) sensor but it had improved spectral and spatial resolution compared with its predecessor the Multispectral Scanner System (MSS) [25]. Only the blue (B), green (G), red (R), near infrared (NIR) and shortwave infrared (SWIR 1 and 2) bands of the
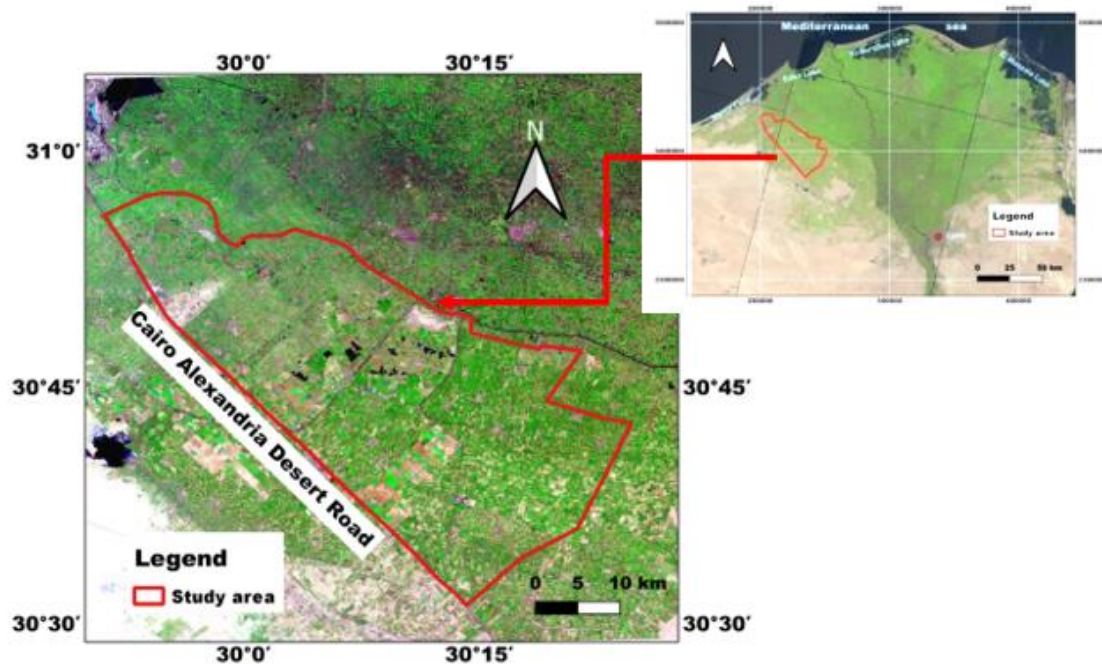

Fig. 1. Location map of the study area (background map Landsat image acquired on 30/9/2020)

images were used in this study. The Landsat data were processed using the Semi-Automatic Classification Plugin (SCP) of the QGIS software. The images were imported, stacked into one multiband (6 bands) image for each date, and subsetted into the geographical extent of the study area.

Subsequently, correlation analyses between the used bands were applied and a modified approach of the data processing recommended by Morgan and Faisal [26] for LULC classification was utilized. The modified approach included firstly, the production of a simple ratio (SR) between blue and shortwave infrared bands as follows:.

$$SR = R_B/R_{SWIR1}$$

Where R refers to band reflectance, and the subscripts refer to a specific spectral band

Then, the soil adjusted vegetation index (SAVI) developed byHuete [27] was applied as follows:.

$$SAVI = ((R_{NIR}-R_R)/(R_{NIR}+R_R+L))\times(1+L)$$

Where R refers to band reflectance, and the subscripts refer to a specific spectral band and L is the soil adjustment factor.

Then, a specific principal component analysis (PCA) on the shortwave infrared bands (PCA$_{sw}$) was conducted. Afterwards, another PCA was implemented on the multiband images (PCA$_{All}$) of each date. Subsequently, the images from the prior processing were stacked to generate a multiband image for each date and these images were used for LULC analysis. Bands computations and the PCA operations were applied using the Semi-Automatic Classification Plugin (SCP) of the QGIS software. Subsequently, the supervised classification with the maximum likelihood classification (MLC) was employed to generate the LULC maps. MLC is considered the most commonly used image supervised classification method which makes use of a discriminate function to allocate pixel to the class with the highest probability based on training data [28]. The spectral separability between each two classes was estimated using the Transformed Divergence separability [29]. Moreover, the overall accuracy of the classified image was examined. It compares how each of the pixels is classified versus the land cover acquired from their corresponding ground truth data and calculated as the percentage of the

correctly classified validation pixels to the total number of pixels in the ground truth data [30].

2.2.2 Moderate Resolution Imaging Spectroradiometer (MODIS)

This study utilized the Terra MODIS MOD16A3GF Version 6.1 evapotranspiration product. These data were generated at the end of each year, representing the sum of daily values within the defined year based on the Penman-Monteith equation. This equation includes inputs from meteorological reanalysis data and MODIS remotely sensed data products, including vegetation property dynamics, albedo, and land cover [31]. The data were available in the Hierarchical Data Format (HDF) via the internet at https://earthexplorer.usgs.gov (accessed on February, 2023). Nevertheless, the data were only available from 2000 and was collected from 2000 to 2021. They were downloaded and imported into the QGIS software, converted into Tiff format and subsetted to the geographical extent of the study area.

2.3 Meteorological Data

The meteorological data used in this study were obtained from NASA's Prediction Of Worldwide Energy Resource (POWER) project. These data were freely available for download at https://power.larc.nasa.gov/data-access-viewer (accessed on February 2023). They had a grid resolution of 0.5 arc degree longitude by 0.5 arc degree latitude [32]. The POWER project collects its data from NASA sources such as World Climate Research Program, Global Energy and Water Cycle Experiment, Surface Radiation Budget Project and the Clouds & the Earth's Radiant Energy System projects at NASA LaRC, as well as the Global Modeling and Assimilation Office at the Goddard Space Flight Center [33]. To evaluate the climate change trends in the studied area the data was collected from 1984 to 2021 including annual mean values of temperature, relative humidity and wind speed as well astotal annual precipitation.

The simple linear regression was applied between the time and each of the climate variables considering the time as independent and the climate variable as the dependent. The simple linear regression is the most commonly considered analysis method when examining the relationship between a quantitative outcome and a single quantitative explanatory variable

[34].Moreover the anomalies which represented the departure from the average values were also calculated. It allows more accurate descriptions than actual climatic parameter and provides a frame of reference that allows easier analysis [35].

3. RESULTS AND DISCUSSION

3.1 Land use/ Land Cover Classification

Based on fieldwork and knowledge of the studied area, five LULC classes were identified. They included vegetation, fallow soils, urban area, barren land and water/fish ponds classes. The correlation matrix between the Landsat bands used in this study was developed for the three used images. Within this matrix the correlation coefficient between the reflectance of each pair of satellite bands is computed for each pixel in the images.

The results revealed a high correlation (r) between the different bands for all images exceeding 0.90 particularly for those acquired in September 1984 and 2020, with a correlation greater than 0.96. Due to the high correlation between the bands, the modified approach ofMorgan and Faisal [26] was used for LULC classification as described in methodology and thus SR$_{BSW1}$, SAVI, PCA$_{sw}$ and PCA$_{All}$ were developed.

The first PCA$_{sw}$ accounted for 99.6%, 99.5% and 99.9% of the variability of the data of 1984, 2001 and 2020 images, respectively. Similarly, the first PCA$_{All}$ accounted for 99.2%, 94.5% and 98.6% of the variability of the data of 1984, 2001 and 2020

images, respectively. Therefore, only the first PCA$_{sw}$ and first PCA$_{All}$ were used. These images were stacked to create four-band images for each date, which were then used in LULC classification.

Thirty five training samples were used to train the MLC classifier to differentiate the LULC classes in the study area. Regions of interest for each image were created in the QGIS software to represent the training data. The separability of the training sets was evaluated to examine the separability between each two classes and the Transformed Divergence measures for each two classes showed a separability of more than 1.8, indicating good separability between classes. The training samples were employed to train the MLC classifier to categorize the LULC classes of the study area on the three dates (Fig. 2). The results showed that the overall accuracy was 91.4%, 82.5% and 82.8% for the images acquired on 1984, 2001 and 2020, respectively.

The results of the classification showed that that the barren land was the major LULC class in 1984 covering about 53% of the studied area and gradually decreased to reach only 4.8 % of the studied area in 2020. Furthermore, the urban area increased from none in 1984 to 8.1% of the studied area in 2001, and to 13.8% in 2020 (Table 1). The agricultural area, including fallow soils and vegetation classes, increased from 46.7% in 1984 to 64.4% in 2001 and almost doubled to 80.3% in 2020. The water/fishponds class increased from 0.4% in 1984, mainly representing water ponds, to 1.9% in 2001 and mostly representing fishponds; however, it decreased to 1.1% in 2020.
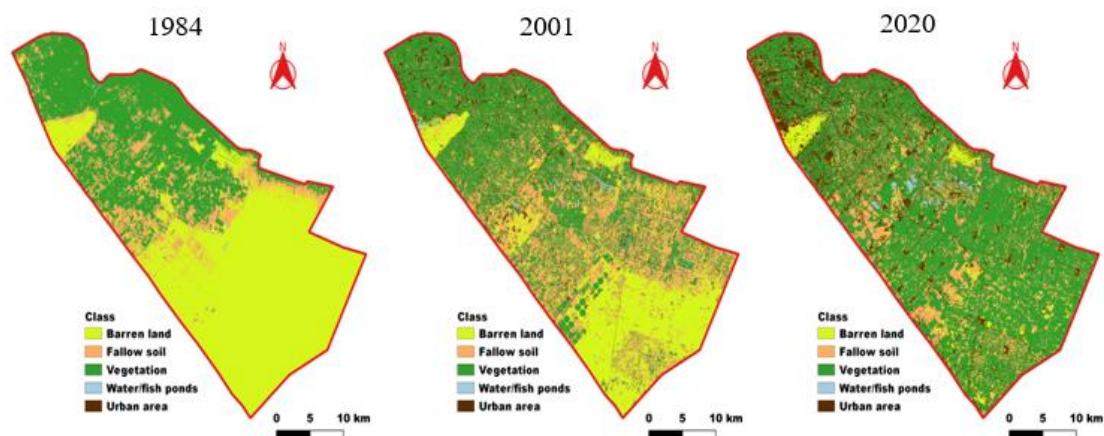

Fig. 2. Land use/ land cover classification

Table 1. Acreage of the land use/ land cover classes of the studied area

Class	1984		2001		2020	
	Km^2	%	Km^2	%	Km^2	%
Barren land	589.0	52.9	285.6	25.7	53.1	4.8
Fallow soils	144.3	13.0	305.7	27.5	201.0	18.1
Vegetation	375.1	33.7	410.9	36.9	692.9	62.3
Water/ fish ponds	4.4	0.4	20.6	1.9	12.2	1.1
Urban area	0.0	0.0	90.0	8.1	153.6	13.8
Total	1112.8	100.0	1112.8	100.0	1112.8	100.0

3.2 LULC Change Detection

Tables 2 show the post-classification change detection within each mapping unit from 1984 to 2001 (hereafter referred to as P1) and from 2001 to 2020 (hereafter referred to as P2), respectively. On the other hand, Fig. 3 A and B represented the overall change to each mapping unit. The unchanged classes accounted for 59.9% and 61.6% of the studied area in P1 and P2, respectively. The most notable change was from barren land to agricultural area, covering 27.3% of the studied area and 51.6% of the barren land class in P1. This trend continued in P2 with 19.2% of the studied area and 74.9% of the barren land class changing to agricultural area.

Additionally, conversion from agricultural area to urban area occurred similarly in both periods representing 12.9% and 12.5% of the agricultural area in P1 and P2, respectively. Changes to agricultural area mainly occurred in the southern part of the studied area in both periods, while the northern part had an increase in urban area

(represented by settlements). To evaluate the impact of climate change on ET, only the area that remained unchanged as agricultural area in P1 and P2 were considered, and all other classes were masked. This agricultural area covered 326.3 Km^2 and 29.3% of the total studied area (Fig. 3 C).

3.3 Meteorological Data Analyses

The annual mean temperature, wind speed, humidity and annual precipitation from 1984 to 2021 were plotted verses time and the linear trends were presented graphically in Fig. 4. The average annual temperature within the study period was 21.8 °C while the highest mean temperature was recorded in 2010 and reached 23.05 °C and the lowest was recorded in 1992 and reached 20.77 °C. The average annual wind speed was 2.8 m/s while the fastest wind speed was 2.88 m/s in 2019 and the slowest was 2.76 m/s in 2014. The highest RH was in 2020 and reached 59.19 % while the lowest was in 2010and was 51.50 % with a mean RH of 55.1 %. The average total amounts of precipitation
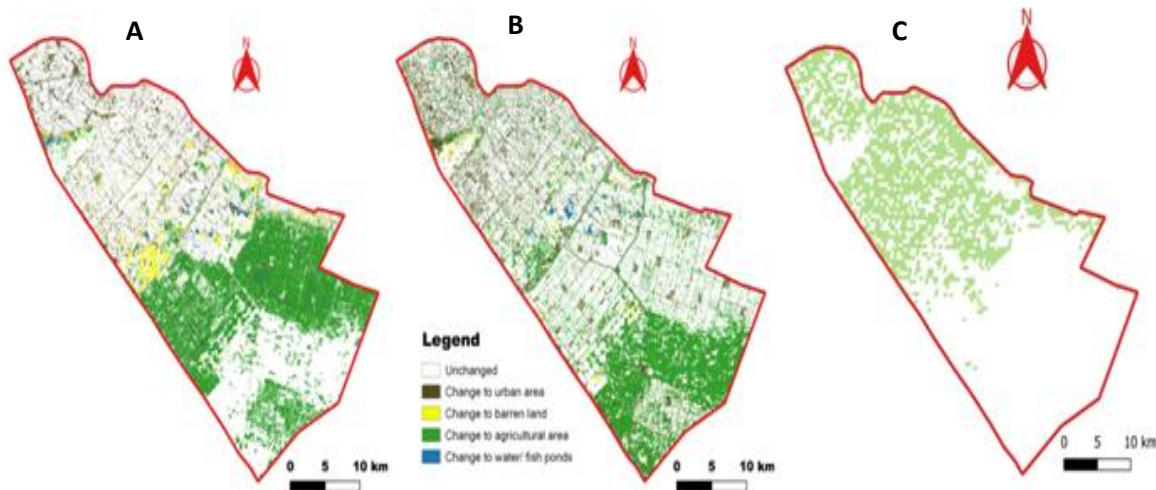

Fig. 3. LU/LC change (A:P1, B:P1 and C: Unchanged vegetation area from P1 to P2)

Table 2. Land use/ land cover change from 1984-2020

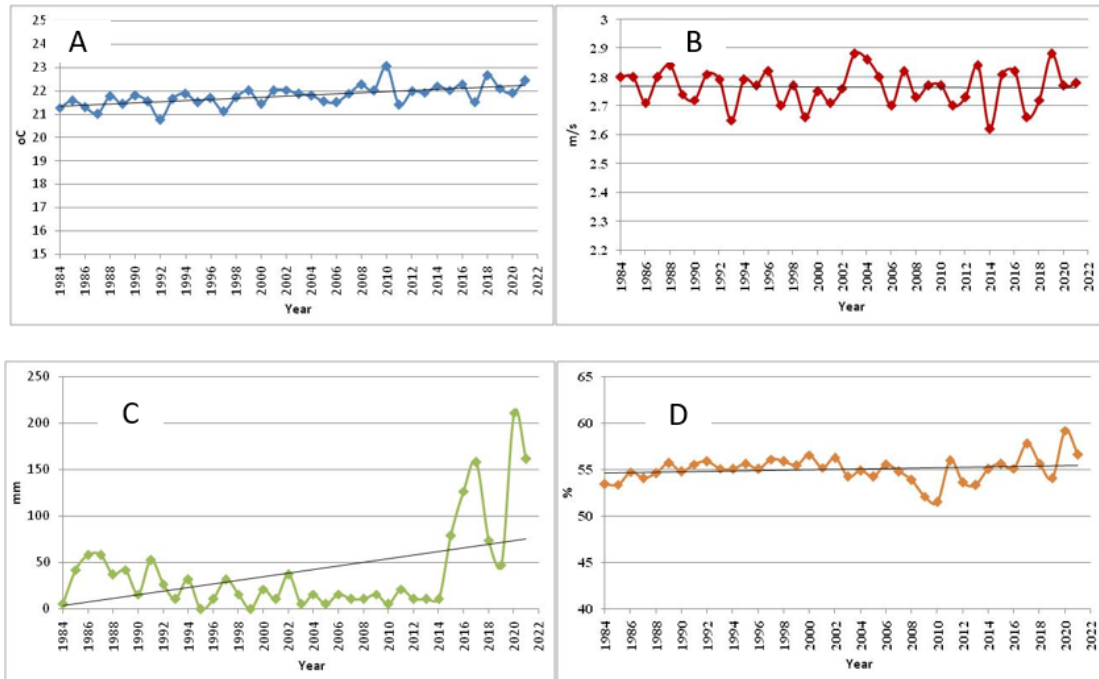| LULC class (from)	Class change (to)	LULC class change from 1984 to 2001		LULC class change from 2001 to 2020	
		Area Km^2	% of class	Area Km^2	% of class
Barren land	Unchanged	254.9	43.3	40.9	14.3
	Agricultural area	304.0	51.6	213.8	74.9
	Water / fish ponds	8.2	1.4	1.0	0.3
	Urban area	21.9	3.7	29.9	10.5
	Total class	589.0	100.0	285.6	100.0
Agricultural area	Unchanged	410.7	79.1	610.6	85.2
	Barren land	30.5	5.9	11.6	1.6
	Water / fish ponds	11.1	2.1	5.1	0.7
	Urban area	67.1	12.9	89.3	12.5
	Total class	519.4	100.0	716.6	100.0
Water / fish ponds	Unchanged	1.4	29.7	4.1	19.9
	Barren land	0.2	5.3	0.1	0.5
	Agricultural area	1.9	43.9	12.0	58.1
	Urban area	0.9	21.1	4.4	21.5
	Total class	4.4	100.0	20.6	100.0
Urban area	Unchanged	---	---	29.7	33.0
	Barren land	---	---	0.5	0.6
	Agricultural area	---	---	57.8	64.2
	Water / fish ponds	---	---	2.0	2.3
	Total class	---	---	90.0	100.0
Total	---	1112.8	---	1112.8	---

Fig. 4. Annual mean temperature (A) , wind speed (B), relative humidity (C) and annual precipitation (D) and their linear trend form 1984 - 2021

were 39.5 mm/year and it was also observed that starting in 2015 there was abnormal increase in the amounts of precipitation that reached its highest in 2020, where it was 21.94 mm/year and the noticeable increase from 2015 to 2021 in precipitation caused the trend to be increasing

throughout the study period, which otherwise would be taking a decreasing trend.

There was an increased warming trend by a rate of 0.024 °C which is less than the increase in global average temperature [35]. The increased trend in relative humidity was by 0.023% while there was no change in the annual wind speed. On the other hand, the highest increase trend was reported for precipitation, which reached 1.927 mm.

The correlation analysis between the climate variables revealed that there was a very weak correlation between each two variables (less than 0.1) except between annual total precipitation and mean RH which had a positive moderate correlation of 0.54. As the relative humidity increases it leads to the formation of clouds and subsequent precipitation [36].

Furthermore, the anomalies in annual change of the mean temperature, wind speed, humidity, and annual precipitation were plotted against time and their linear trends are represented in Fig. 5. In this figure, the linear trend represented by the slope of the regression line of time (independent) versus (climate parameter) refers to the magnitude of rise or fall of the studied

climatic parameter. In case of mean annual temperature, relative humidity and annual total precipitation the slope was evidently increasing from year to year, while it was constant in case of wind speed. It was also observed that the trend line in the case of temperature almost divided the series into two equal periods, the first from 1984 to 2003 with mostly negative values and the second from 2003 to 2021 with mostly positive values, indicating coldness relative to the mean value in the first period and warmness in the second. On the other hand, the annual precipitation was affected by the enormous increase from 2015 to 2021 as previously mentioned, which caused the trend to be increasing instead of decreasing. The relative humidity took a wavy trend of decreasing and increasing from the mean value.

3.4. Impact of Climate Change on ET

The MODIS ET products were available from 2000 to 2021 and the agricultural area since 1984 were used to extract the ET values within this area to minimize the impact of LULC change on ET values as the vegetation pattern in this agricultural area has undergoneminimal alteration since 1984. The minimum, maximum and average ET annual values throughout this
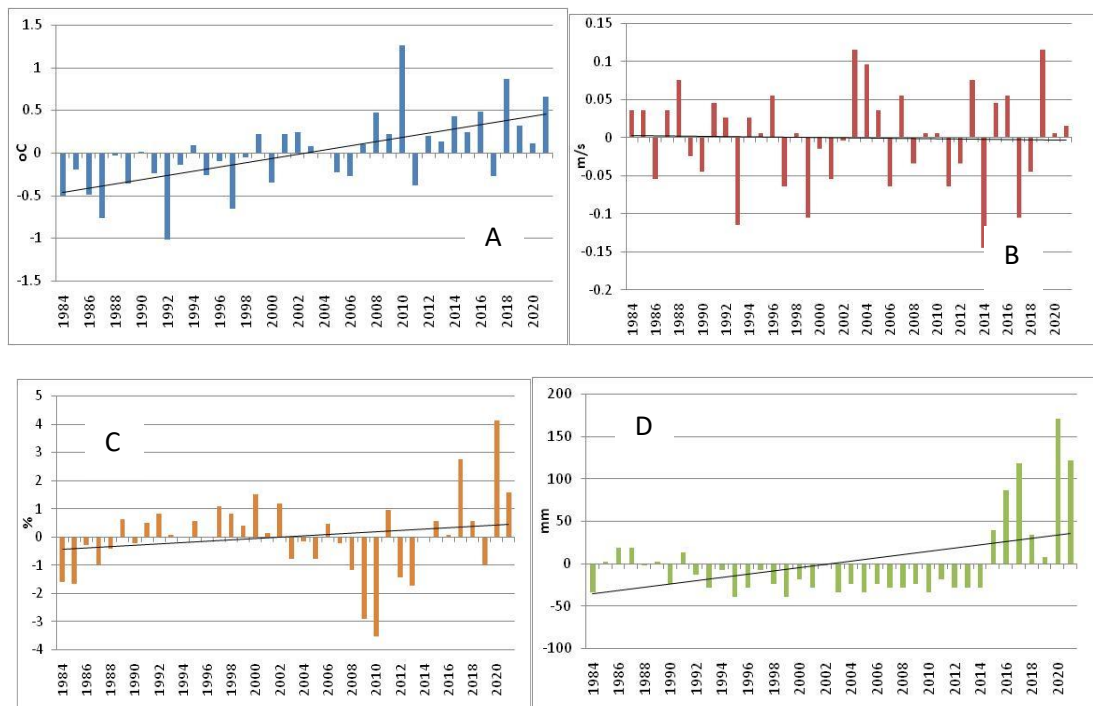

Fig. 5.the anomalies of annual mean temperature (A), wind (B), relative humidity (C) and annual precipitation (D) and their linear trend form 1984 – 2021
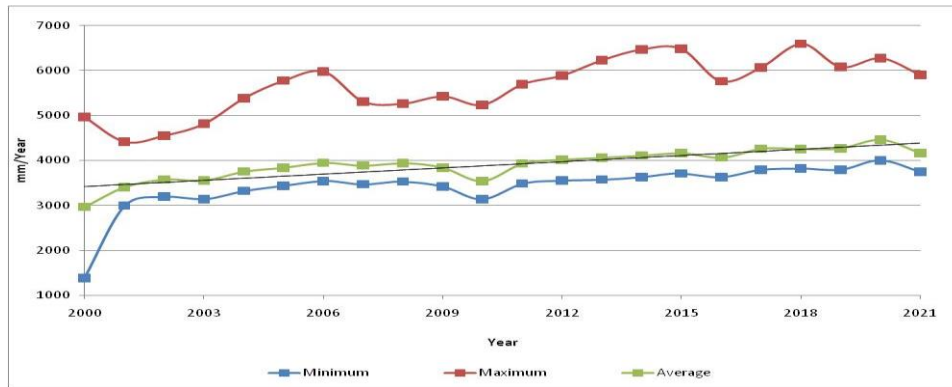
Fig. 6. Summary of ET annual values in the studied agricultural area

studied agricultural area from 2000 to 2021 are shown in figure 6. The lowest ET value was in 2000 and reached 1377 mm/year while the highest was in 2018 and reached 6592 mm/year and the average ET value was 3906 mm/year. There was an increase trend in annual ET reaching 48.2 mm/year accounting for 2% of the average annual ET. There was a strong correlation between time and average ET reaching r^2 of 0.80. Nevertheless, there was a very weak correlation between the mean annual ET and the studied climatic parameters (r^2 less than 0.1) except for the annual total precipitation, which had a moderate correlation ($r^2 = 0.36$). Similar results were obtained by Nagler et al. [37] in vegetated areas in a semiarid watershed. They suggested that transpiration is the dominant process controlling ET as an increase in precipitation would increase the yield and consequently the transpiration.

The studied agricultural area was classified into six classes according to the ET annual values

and examples of these maps are shown in Fig. 7. On the other hand, the area covered by each class and their changes trend is shown in Fig. 8. The data revealed that the first two classes (A: 1000-2000 and B: 2000-3000 mm/year) had a descending trend of 1.12 and 6.21, respectively, while the other four classes (C: 3000-4000, D: 4000-5000, E: 5000-6000 and F: 6000-7000 mm/year) had an increasing trend of 3.87, 3.09, 0.34 and 0.02, respectively. The largest area covered by class A was in 2000 and covered 31.6 Km^2, while the lowest was in 2020 and covered 0.4 Km^2. The largest area covered by class B was 2001 covering 173.7 Km^2 and the lowest in 2020 covering 20.4 Km^2. The area covered by class C ranged between 121.5 Km^2 in 2001 to 233.3 Km^2 in 2021 while, the area covered by class D ranged between 6.0 Km^2 in 2001 to 105 Km^2 in 2020. The ET more than 5000 mm/year started to appear in 2004 where it covered 0.9 Km^2 and increased to reach 10.7 Km^2 in 2020.
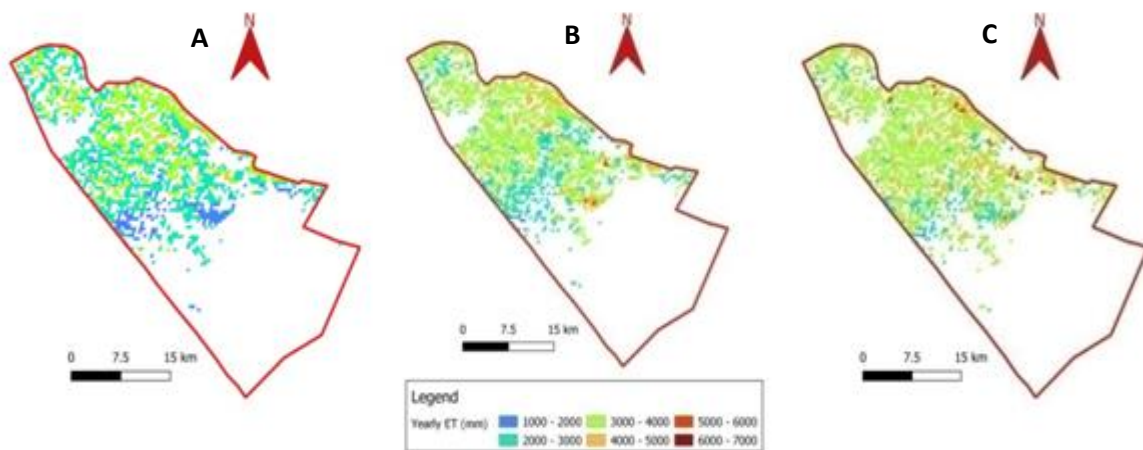

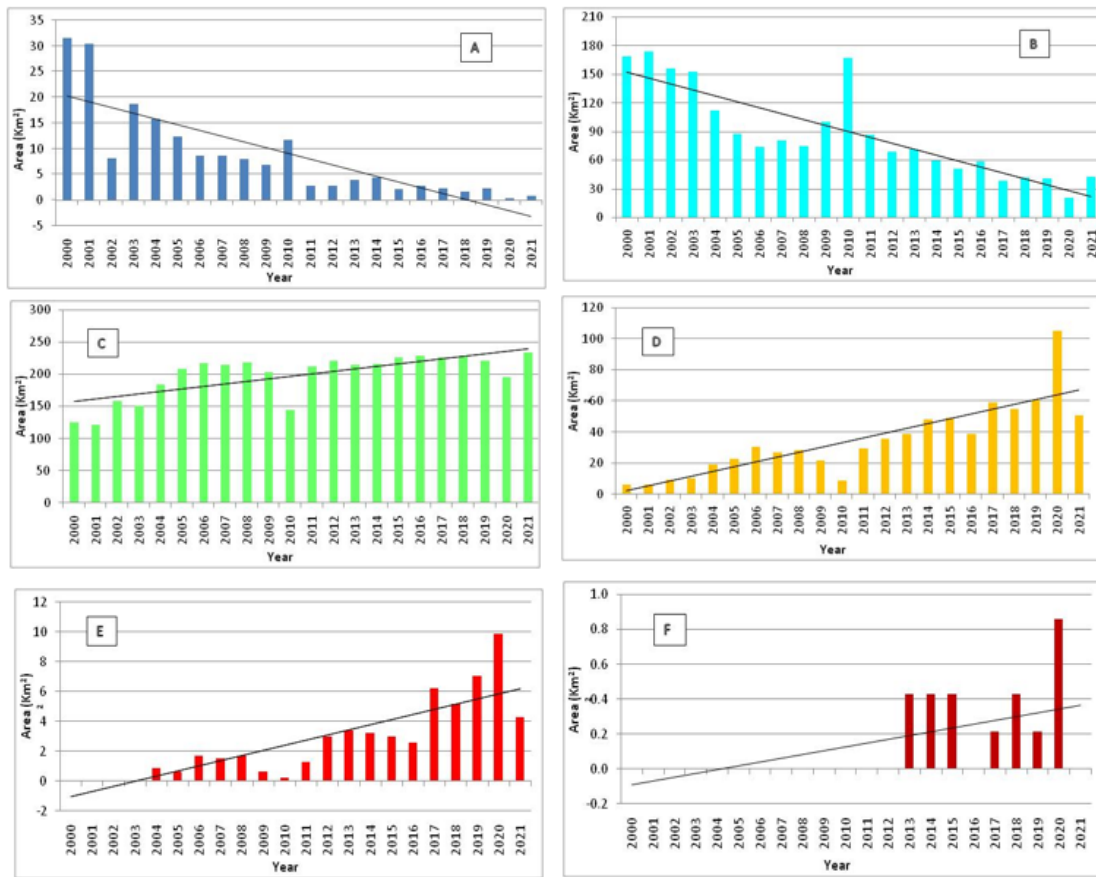**Fig. 7. Annual ET classification in A: 2000, B: 2011 and C: 2021**

Fig. 8. Acreage of the annual ET classes

4. CONCLUSION

This study assessed climate change trends and spatiotemporal variations of ET in a selected area in El-Beheira Governorate, Egypt. The LULC classification revealed that the barren land was the major LULC class in 1984 but due to reclamation projects that took place in the area, this area decreased to less than 5% of the studied area. Contrary, due to the same reason the agricultural area and urban area increased gradually from 46.7 and 0.0 % in 1984 to 80.3 and 13.8 % of the studied area in 2020, respectively. Therefore, the LULC change detection revealed that most of the change was from barren land to agricultural area and the area that remained unchanged as agricultural area throughout this period was considered for evaluating the spatiotemporal variations of ET and represented 29.3% of the total studied area.

The study area underwent an increased trend in temperature, relative humidity and precipitation while there was no change in the annual wind speed. Similarly, the trend of anomalies change of the temperature, humidity and precipitation increased from year to year, while it was constant in case of wind speed. No correlation was found between the climatic parameters except between RH and precipitation.

Increased temperatures, alterations in precipitation patterns, and decreases in water availability, may all lead to decreased agricultural output and consequently affects food security. Therefore, the agricultural practices changes in the study area are recommended to overcome such impacts, including modifications in crop management as well as enhancements in irrigation systems.

There was an increasing trend of ET values in the selected agricultural area. Furthermore, there was a decrease in the area of ET less than 3000 mm/year and increase in the area above this value, especially the area of ET from 3000 – 5000 mm/year. The increase trend in ET indicate an increase in the required irrigation water as

most of these water will be used by plant in ET and only a small amount is used in the physiological growth and metabolism [38]. Moreover, there was no correlation between the ET and the studied climatic parameters except for precipitation which had a moderate correlation with ET.

Further research is recommended on the impacts of climate change on ET utilizing finer spatial resolution remote sensing data. Despite that MODIS ET products have the advantage of continuous ET monitoring at a fine temporal resolution, its coarse spatial resolution is not suitable for small-scale applications due to the considerable spatial variability in land cover within a pixel. Therefore, it is recommended to emply fusion between MODIS data and fine resolution data such as Lanadsat data to produce data suitable for small scale ET data.

COMPETING INTERESTS

Authors have declared that no competing interests exist.

REFERENCES

1. IPCC. Climate Change. The Physical Science Basis. Contribution of Working Group I to the Fourth Assessment Report of the Intergovernmental Panel on Climate Change [Solomon, S., D. Qin M. Manning Z. Chen M. Marquis, KB. Averyt M. Tignor, HL. Miller (eds.)]. Cambridge University Press, Cambridge, United Kingdom and New York, NY, USA. 2007.

2. IPCC. Summary for Policymakers. In: Climate Change 2023: Synthesis Report. Contribution of Working Groups I, II and III to the Sixth Assessment Report of the Intergovernmental Panel on Climate Change [Core Writing Team, H. Lee and J. Romero (eds.)]. IPCC, Geneva, Switzerland; 2023.
   DOI:10.59327/IPCC/AR6-9789291691647.001

3. Andaryani S, Nourani V, Abbasnejad H, Koch J, Stisen S, Klöve B, Haghighi AT. Spatio-temporal analysis of climate and irrigated vegetation cover changes and their role in lake water level depletion using a pixel-based approach and canonical correlation analysis. Science of the Total Environment. 2023;873:162326.

4. Abtew W, Melesse A. Climate Change and Evapotranspiration. In: Evaporation and Evapotranspiration. Springer, Dordrecht; 2013.
   DOI: 10.1007/978-94-007-4737-1_13
   Accessed on: May 2023.

5. Makar RS, Shahin SA, El-Nazer M, Wheida A, Abd El-Hady M. Evaluating the impacts of climate change on irrigation waterrequirements.Sustainability.2022;14(22):14833.

6. Basso B, Martinez-Feria RA, Rill L, Ritchie JT. Contrasting long-term temperature trends reveal minor changes in projected potential evapotranspiration in the US Midwest. Nature Communications, 2021;12:1476.
   DOI: 10.1038/S41467-021-21763-7

7. Tijjani S B, Giri S, Sean A, Woznicki S A. Quantifying the potential impacts of climate change on irrigation demand, crop yields, and green water scarcity in the New Jersey Coastal Plain. Science of the Total Environment.2022;838:156538.

8. Santos CAG, da Silva RM, Silva, AM, Neto RMB. Estimation of evapotranspiration for different land covers in a Brazilian semi-arid region: A case study of the Brígida River basin, Brazil. Journal of South American Earth Sciences. 2017;74:54-66.

9. Minacapilli M, Consoli S, Vanella D, Ciraolo G, Motisi A. A time domain triangle method approach to estimate actual evapotranspiration: Application in a Mediterranean region using MODIS and MSG-SEVIRI products. Remote Sensing of Environment.2016;174:10-23.

10. Chehbouni A, Escadafal R, Duchemin B, Boulet G, Simonneaux V, Dedieu G, Sobrino JA. An integrated modelling and remote sensing approach for hydrological study in arid and semi-arid regions: The SUDMED programme. International Journal of Remote Sensing.2008; 29: 5161-5181.
    DOI:10.1080/01431160802036417

11. Zhang C, Brodylo D, Rahman M, MdRahman A, Douglas T A, Comas X. Using an object-based machine learning ensemble approach to upscale evapotranspiration measured from eddy covariance towers in a subtropical wetland. Science of the Total Environment.2022;831: 154969.

12. [12] He M, Kimball, J S, Yi Y, Running SW, Guan K, Moreno A, Wu X, Maneta M. Satellite data-driven modeling of field scale evapotranspiration in croplandsusing the

MOD16 algorithm framework. Remote Sensing of Environment.2019;230:111201.

13. Li G, Zhang F, Jing Y, Liu Y, Sun G. Response of evapotranspiration to changes in land use and land cover and climate in China during 2001–2013. Science of the Total Environment.2017;596:256-265.

14. Ke Y, ImJ, Park S, Gong H. Spatiotemporal downscaling approaches for monitoring 8-day 30 m actual evapotranspiration. ISPRS Journal of Photogrammetry and Remote Sensing.2017;126: 79–93.

15. Dash S S, Sahoo B, Raghuwanshi NS. How reliable are the evapotranspiration estimates by Soil and Water Assessment Tool (SWAT) and Variable Infiltration Capacity (VIC) models for catchment-scale drought assessment and irrigation planning?.Journal of Hydrology.2021;592: 125838.

16. Xue W and Ko J. Radiation estimation and crop growth trajectory reconstruction by novel algorithms improve MOD16 evapotranspiration predictability for global multi-site paddy rice ecosystems. Journal of Hydrology.2022;612:128204.

17. Vorosmarty C J, Green P, Salisbury J, Lammers R B. Global water resources: vulnerability from climate change and populationgrowth. Science.2000;289(5477):284-288.

18. Li Y, Liu Y, Bohrer G, Cai Y, Wilson A, HuT, Wang Z, Zhao K. Impacts of forest loss on local climate across the conterminous United States: Evidence from satellite time-series observations. Science of the Total Environment.2022;802:149651.

19. Gashaw T, Tulu T, Argaw M, Worqlul A W. Modeling the hydrological impacts of land use/land cover changes in the Andassa watershed, Blue Nile Basin, Ethiopia. Science of the Total Environment.2018;619:1394-1408.

20. Goyal RK. Sensitivity of evapotranspiration to global warming: A case study of arid zone of Rajasthan (India). Agricultural water management. 2004;69(1):1-11.

21. Snyder R L, Moratiel R, Zhenwei S, Swelam A, Jomaa I, Shapland T. Evapotranspiration response to climate change. ActaHortic.2011;922:91-98.
DOI: 10.17660/ACTAHORTIC.2011.922.11

22. Sarkar S, Sarkar S. A review on impact of climate change on evapotranspiration.The Pharma Innovation Journal. 2018; 7(11):387-390.

23. Ebaid H M, Farag, H A, El Falaky AA. Using GIS and Remote Sensing Approaches to Delineate Potential Areas for Runoff Management Applications in Egypt. International Journal of Environmental Scince and Engineering. 2016;7:85- 93.

24. RoyD P, Kovalskyy V, Zhang HK, Vermote EF, Yan L, Kumar SS,Egorov A. Characterization of Landsat-7 to Landsat-8 reflective wavelength and normalized difference vegetation index continuity. Remote Sens. Environ. 2016;12(185):57-70.
DOI: 10.1016/j.rse.2015.12.024

25. Chen F, Lou S, Fan Q, Wang C, Claverie M, Wang C, Li J. Normalized difference vegetation index continuity of the Landsat 4-5 MSS and TM: investigations based on simulation. Remote Sensing. 2019;11(14):1681.

26. Morgan R S, Faisal M. Improving land use/land cover classification utilizing a hybrid method of decision trees and artificial neural networks. Bioscience Research. 2018;15(4):4049-4060.

27. Huete A R. soil-adjusted vegetation index (SAVI). Remote sensing of environment.1988;25(3): 295-309.

28. Ahmad A, Quegan S. Analysis of maximum likelihood classification technique on Landsat 5 TM satellite data of tropical land covers. In 2012 IEEE International Conference on Control System, Computing and Engineering. 2012:280-285.

29. Bhaskaran S, Paramananda S, Ramnarayan M. Per-pixel and object-oriented classification methods for mapping urban features using Ikonos satellite data. Appl. Geogr. 2010;(4):650-665.

30. Rwanga SS, Ndambuki JM. Accuracy assessment of land use/land cover classification using remote sensing and GIS. International Journal of Geosciences.2017;8(04):611.

31. Running SW, Mu Q, Zhao M, Moreno A. User's Guide MODIS Global Terrestrial Evapotranspiration(ET) Product(MOD16A2/A3 and Year-end Gap-filled MOD16A2GF/A3GF) NASA Earth). Observing System MODIS Land Algorithm (For Collection 6.1); 2021.

Available:https://www.ntsg.umt.edu/project/ modis/user- guides/mod16c61usersguidev11mar11202 1.pdf
Accessed on: May 2023.

32. Sparks AH. Nasapower: A Nasa Power global meteorology, surface solar energy and climatology data client for R. Journal of Open Source Software. 2018; 3(30):1035.

33. Akram H, Levia D F, Herrick J E, Lydiasari H, Schütze N. Water requirements for oil palm grown on marginal lands: A simulation approach. Agricultural Water Management. 2022;260:107292.

34. Seltman H. Experimental Design and Analysis;2018.
Available:https://www.stat.cmu.edu/~helt man/309/Book/Book.pdf
Accessed on: May 2023.

35. Al-Muhyi AH. The study of climate change, Using statistical analysis case study temperature Variation in Basra.International Journal of Academic Research.2016;3:10-23.

36. Olusanya J. Variation of rainfall and humidity in Nigeria. Journal of Environment and Earth Science.2014 4(2):29.

37. Nagler PL, Glenn EP, Kim H, Emmerich W, Scott RL, Huxman TE, Huete AR. Relationship between evapotranspiration and precipitation pulses in a semiarid rangeland estimated by moisture flux towers and MODIS vegetation indices. Journal of Arid Environments.2017;70(3): 443-462.
Available:https://doi.org/10.1016/j.jaridenv. 2006.12.026

38. Ren R, Liu T, Ma L, Fan B, Du Q, Li J. Irrigation based on daily weighted evapotranspiration affects yield and quality of oriental melon.ScientiaHorticulturae.2021;275:109 714.